

## ORIGINAL RESEARCH

American Society  
of Plant Biologists  
Cultivating a better future through plant biology research

WILEY

# Real-time whole-plant dynamics of heavy metal transport in *Arabidopsis halleri* and *Arabidopsis thaliana* by gamma-ray imaging

Kaisa Kajala<sup>1,2</sup> | Katherine L. Walker<sup>3</sup> | Gregory S. Mitchell<sup>3</sup> | Ute Krämer<sup>4</sup> | Simon R. Cherry<sup>3</sup> | Siobhan M. Brady<sup>1</sup>

<sup>1</sup>Department of Plant Biology and Genome Center, University of California Davis, Davis, California

<sup>2</sup>Plant Ecophysiology, Institute of Environmental Biology, Utrecht University, Utrecht, The Netherlands

<sup>3</sup>Department of Biomedical Engineering, University of California Davis, Davis, California

<sup>4</sup>Molecular Genetics and Physiology of Plants, Ruhr University Bochum, Bochum, Germany

## Correspondence

Siobhan M. Brady, Department of Plant Biology and Genome Center, University of California Davis, Davis, CA.  
Email: sbrady@ucdavis.edu

## Funding information

Office of Science (BER), U.S. Department of Science; Finnish Cultural Foundation HHMI Faculty Scholar

## Abstract

Heavy metals such as zinc are essential for plant growth, but toxic at high concentrations. Despite our knowledge of the molecular mechanisms of heavy metal uptake by plants, experimentally addressing the real-time whole-plant dynamics of heavy metal uptake and partitioning has remained a challenge. To overcome this, we applied a high sensitivity gamma-ray imaging system to image uptake and transport of radioactive <sup>65</sup>Zn in whole-plant assays of *Arabidopsis thaliana* and the Zn hyperaccumulator *Arabidopsis halleri*. We show that our system can be used to quantitatively image and measure uptake and root-to-shoot translocation dynamics of zinc in real time. In the metal hyperaccumulator *Arabidopsis halleri*, <sup>65</sup>Zn uptake and transport from its growth media to the shoot occurs rapidly and on time scales similar to those reported in rice. In transgenic *A. halleri* plants in which expression of the zinc transporter gene *HMA4* is suppressed by RNAi, <sup>65</sup>Zn uptake is completely abolished.

## KEYWORDS

*Arabidopsis halleri*, metal hyperaccumulation, metal transport, metal uptake, nuclear imaging, single photon emission computed tomography, zinc

## 1 | INTRODUCTION

Most plants actively prevent the accumulation of high levels of metals in their aboveground biomass through a functional network of metal homeostasis, in order to avert toxicity. However, metal hyperaccumulators have developed rare adaptations to their environments and selectively extract specific metals from the soil and accumulate them in their shoots at very high concentrations without incurring symptoms of toxicity (Baker & Brooks,

1989; Frérot et al., 2010). In their natural habitat, metal hyperaccumulator plant species accumulate one or several metalloid elements in their aboveground biomass at concentrations two to three orders of magnitude higher than in leaves of most species on normal soils, and at least one order of magnitude greater than the usual range found in plants from metalliferous soils. (Pollard, Reeves, & Baker, 2014). Metal hyperaccumulation in plants can have commercial applications, including phytostabilization (revegetation of contaminated soils), phytomining (extraction of metals

**Abbreviations:** ICP-AES, Inductively coupled plasma atomic emission spectroscopy; ROI, Region of interest; SPECT, Single photon emission computed tomography.

This manuscript was previously deposited as a preprint at: <https://www.biorxiv.org/content/10.1101/428417v1>

This is an open access article under the terms of the Creative Commons Attribution License, which permits use, distribution and reproduction in any medium, provided the original work is properly cited.

© 2019 The Authors. *Plant Direct* published by American Society of Plant Biologists, Society for Experimental Biology and John Wiley & Sons Ltd.



from plants for their value) or phytoremediation (plant-based remediation of soils).

*Arabidopsis halleri* (formerly known as *Cardaminopsis halleri*) is a metal hyperaccumulator species and a facultative metallophyte, that is, it grows naturally on both metal-contaminated (metalliferous) toxic soils and pristine (non-metalliferous) soils. Zinc (Zn) hyperaccumulation (at least 10,000 µg of Zn per g of dry leaf tissue) in *A. halleri* is species-wide, whereas cadmium (Cd) hyperaccumulation (at least 300 µg of Cd per g of dry leaf tissue) is geographically confined (Bert, Macnair, de Laguerie, Saumitou-Laprade, & Petit, 2000; Bert et al., 2003; Frérot et al., 2010; Pauwels, Frérot, Bonnin, & Saumitou-Laprade, 2006). The molecular mechanisms underlying metal hyperaccumulation in *A. halleri* are only partly understood. Typically  $Zn^{2+}$  and other poorly soluble transition metal cations are mobilized in the soil through acidification of the rhizosphere and the release of organic chelators by the root. These transition metal ions are then taken up into the root symplast through ZIP transporters (ZIP, IRT-like Protein) located in the epidermal plasma membrane (Grotz et al., 1998; Ramesh, Shin, Eide, & Schachtman, 2003). They are then thought to move symplastically from cell to cell and are eventually loaded into the apoplastic xylem through the transporters HEAVY METAL ATPASE 4 (HMA4) and HMA2 (Hussain et al., 2004). A quantitative trait locus for  $Cd^{2+}$  hypertolerance in *A. halleri* was found to map to a chromosomal region containing the HMA4 gene (Courbot et al., 2007). Transgenic *A. halleri* lines in which HMA4 was silenced by RNA interference were employed to demonstrate a key role for HMA4 in Zn and Cd hyperaccumulation as well as Zn and Cd hypertolerance (Hanikenne et al., 2008). In comparison to *A. thaliana*, the strongly enhanced expression of HMA4 in *A. halleri* results from a combination of modified cis-regulatory sequences and copy number expansion (Hanikenne et al., 2008). Transfer of an *A. halleri* HMA4 gene into *A. thaliana* recapitulates Zn partitioning into xylem vessels and the constitutive transcriptional upregulation of Zn uptake system-encoding Zn deficiency-responsive genes including ZIP4 and IRT3 in roots. Other genes associated with metal hypertolerance and/or hyperaccumulation in *A. halleri* include constitutively highly expressed NICOTIANAMINE SYNTHASE (NAS2 and NAS3), METAL TOLERANCE PROTEIN 1 (MTP1) and NATURAL RESISTANCE-ASSOCIATED MACROPHAGE PROTEINS (NRAMP) genes (Hanikenne & Nouet, 2011; Krämer, Talke, & Hanikenne, 2007).

The functional characterization of candidate metal transporters can reveal the molecular mechanisms by which metal hyperaccumulation occurs. Imaging methods can reveal the spatiotemporal dynamics of metal translocation within and between roots and shoots. According to the present model, hyperaccumulation is primarily a consequence of high rates of metal loading into the root xylem, which depletes the metal in the root symplast and secondarily induces elevated rates of metal uptake into the root (Hanikenne et al., 2008; Krämer, 2010). Additional contributions were proposed from chelation in the root symplast (Deinlein et al., 2012), high rates of unloading from the xylem and distribution across leaf tissues where the metal can be stored in mesophyll cells and is present in high amounts in vacuoles (Hanikenne et al., 2008). However, the

## Highlight

We have used gamma-ray imaging to visualize the stark differences in real-time whole-plant dynamics of zinc root-to-shoot transport in heavy metal hyperaccumulating and non-accumulating *Arabidopsis*.

time scale by which metal uptake into the root is followed by root-to-shoot translocation remains unknown. Within the root, mathematical modeling approaches have explored the importance of ZIP regulation, HMA abundance and symplastic transport in the creation of the radial pattern of Zn within primary roots of *A. thaliana* (Claus, Bohmann, & Chavarría-Krauser, 2013). Modeling predicted that Zn transport in the symplast takes place at the same time scale as symplastic transport with Zn carried along the water flow path at the same velocity of water (Claus et al., 2013). Transpiration is thus a key determinant of the rate of this water transport for symplastic, root cell-to-cell transport. The metal must then be loaded into the xylem by the HMA4 transporter to undergo apoplastic transport from the root to shoot. In the hyperaccumulator *A. halleri*, Cd translocation from the external hydroponic medium into the xylem was very rapid: After a 2-hr exposure to Cd, its concentration in xylem sap was 5-fold higher than that in the external solution (Ueno, Iwashita, Zhao, & Ma, 2008). This Cd concentration in xylem sap decreased with increasing the concentration of external Zn suggesting that it is a function of the HMA4 transporter. Based on nuclear magnetic resonance (NMR) and computational modeling of metal speciation by Geochem-PC of xylem sap, Cd was proposed to mainly occur in the free ionic form in the xylem sap.

Invasive methods involving decapitation of plants or detachment of stems have revealed aspects of the dynamics of apoplastic transport once metal is loaded into the xylem. Apoplastic transport of water in xylem of *A. thaliana* occurs within 30 min (Park et al., 2014), while xylem sap of *A. halleri*, collected after exposure to high Cd, accumulates Cd within the same time scale of 30 min (Ueno et al., 2008). At the single cell or tissue level, Förster resonance electron transfer (FRET) imaging in root cells revealed a high-affinity, low-capacity uptake system, a low-affinity, high-capacity uptake system as well as of a mechanism allowing  $Zn^{2+}$  release from internal cell stores in *A. thaliana* (Lanquar et al., 2014). Synchrotron-based techniques revealed that high concentrations of Cd were located in the vascular system of both the hyperaccumulator *A. halleri* and the non-accumulator, *A. lyrata* in the vascular system of the midrib and in secondary veins. The two species differ in the extent of their accumulation of Cd in the mesophyll, with *A. halleri* showing enriched levels relative to *A. lyrata* (Isaure, Fayard, Sarret, Pairis, & Bourguignon, 2006).

To complement these often spatially narrow or invasive studies, whole plant imaging enables direct large-scale material transport studies, addressing spatiotemporal transport within the context of the entire intact plant, from root to shoot for a period of up to



several days. Here, we use a high-sensitivity uncollimated detector single photon emission computed tomography (SPECT)-type imaging system (UCD-SPI (Walker, Judenhofer, Cherry, & Mitchell, 2015)), to study Zn metal transport in a hyperaccumulator, *A. halleri*, and in a non-accumulator *A. thaliana*. We further examine the influence of the HMA4 transporter on Zn transport in *A. halleri* by use of an HMA4 knockdown line.

## 2 | MATERIALS AND METHODS

### 2.1 | Plant material and growth conditions

All plants were cultivated in a growth chamber with a 16 hr:8 hr light:dark cycle at 22°C and 50%–75% humidity with a light intensity of 100  $\mu\text{mol m}^{-2} \text{s}^{-1}$ . We used *A. thaliana* (accession Columbia [Col-0]), *A. halleri* (LAN 5, Langelsheim, Germany), and *AhHMA4-RNAi A. halleri* (Line 4.2.1, Langelsheim, Germany) (Hanikenne et al., 2008). Seeds of *A. thaliana* Col-0 were grown to an age of 18 days on a mix of vermiculite and sand. In this study, 18-day-old plants were transferred from vermiculite and sand (3:1. Perlite:sand) to a hydroponic Hoagland nutrient solution, pH5.8, adjusted with KOH (Becher, Talke, Krall, & Krämer, 2004) but omitting  $\text{ZnSO}_4$ . Zn concentration in this low-Zn medium lacking any added Zn was measured to be 0.12  $\mu\text{M}$  (inductively coupled plasma-atomic emission spectrometry (ICP-AES), UC Davis Analytical Lab). The hydroponic growth was conducted in Magenta vessels (GA-7, Sigma Aldrich), each plant in an individual vessel, on a mesh square suspended over 150 ml of growth medium. *A. halleri* plants were initially grown in Sunshine Mix (3:1 soil:vermiculite). Vegetatively growing *A. halleri* plants were replicated via cuttings and grown in hydroponics. The cuttings were first allowed to root on 1x SensiGrow, prepared according to the manufacturer's recommended working concentration (Advanced Nutrients, USA) nutrient solution for 14 days, before being transferred to Hoagland nutrient solution without Zn. The hydroponic solutions were changed every 4–5 days. Both *A. halleri* and *A. thaliana* plants were grown on Hoagland solution without Zn for 19–21 days prior to imaging to acclimate to Zn deprivation. Both *A. thaliana* and *A. halleri* were at mature vegetative growth stage during the imaging experiments.

### 2.2 | Imaging protocol and conditions

Zn isotope was obtained from the National Isotope Development Center (Oak Ridge National Laboratory), in the form of  $\text{ZnCl}_2$  in solution. The half-life of  $^{65}\text{Zn}$  is 243.9 days, and its primary gamma-ray decay product is of energy 1,116 keV (51% branching ratio). A small positron emission branching ratio of 1.4% also exists.

Plants were transferred from the growth chamber to the imaging laboratory prior to imaging in batches of three where they grew during the time it took to image them. The imaging laboratory light level was 12  $\mu\text{mol m}^{-2} \text{s}^{-1}$  PAR, with a light:dark cycle of 10 hr:14 hr, and was at temperature of 20°C. Prior to imaging, each plant was transferred from the low-Zn Hoagland solution into a solution with

radioactive Zn and 1  $\mu\text{M}$   $\text{ZnSO}_4$ . The plants were incubated in a centrifuge tube containing 50 mL of Hoagland solution with 1  $\mu\text{M}$   $\text{ZnSO}_4$ , to which 200  $\mu\text{Ci}$  of the  $^{65}\text{Zn}$  had been added. Each plant was held in a plastic funnel to avoid direct contact of the plant shoot with the radioactive solution – roots were in the spout and the shoot in the funnel mouth. The funnel was placed in the centrifuge tube and incubated in the  $^{65}\text{Zn}$  solution for 60 min, with the fluid level coming to the full level of the funnel spout to fully immerse the roots. To avoid generating a large amount of radioactive waste all plants were incubated in the same tube. For the first plant, the  $^{65}\text{Zn}$  concentration was 7.2 nM and for the final plant the  $^{65}\text{Zn}$  concentration was 5.6 nM, corresponding to an activity range of 200  $\mu\text{Ci}$  to 150  $\mu\text{Ci}$  in the 50 mL tube, as determined by a calibrated well counter (Capintec, Inc., Florham Park, NJ). The uptake into each plant was typically 4 to 5  $\mu\text{Ci}$ .

Following incubation, each plant was rinsed through three washes of Hoagland solution (with 1  $\mu\text{M}$   $\text{ZnSO}_4$ ) to remove any (non-uptaken) radiolabeled media remaining on the root surface. This was performed with the plant still in the funnel and fresh 50 mL centrifuge tubes. Each rinse was of 20 s, during which the plant was gently swirled in the tube. The rinsing tubes were measured for activity rinsed off of the plant roots and only a small fraction was ever present. Final rinsing for each plant was always performed with a fresh solution. Rinsing solutions were one of the larger components of radiological waste which was generated. The imaging was carried out on Hoagland solution with 1  $\mu\text{M}$   $\text{ZnSO}_4$ .

For gamma ray imaging on the UCD-SPI system, the plants were carefully removed from the funnel and gently constrained with a holder of two 10 cm  $\times$  15 cm pieces of thin transparent plastic, spaced to be separated by 2 cm. The narrow holder constrained the plant leaves to be close to the imaging system and to have the entire plant roots and shoot to be within the system field of view. The holder contained the growth media at a level which completely covered the roots, a few cm below the top opening of the holder. Most of the leaves extended above the holder opening. Only one of the detector heads of the system was used in order to provide better monitoring of the plant condition throughout the imaging process. Plants were imaged continuously for a period of several hours until the gamma ray spatial distribution reached a steady state. Time periods of imaging ranged from 20 hr to 70 hr for the 11 plants.

Data were collected in files recording positions and energies of up to  $8 \times 10^6$  gamma ray events detected by the system. Given the efficiency and sensitivity of the system, this corresponded to a time extent of 20 min for the larger plants with high Zn uptake, to multiple hours for the somewhat smaller *A. thaliana* plants. The data files were used as the time points for subsequent analysis. For each plant, two non-overlapping regions of interest (ROIs) of area 1,280  $\text{mm}^2$  (16 by 20 pixels of detector, each of dimension 2 by 2  $\text{mm}^2$ ) were defined on the detector area, corresponding to the roots and to the leaves of the plant. Total counts recorded in each area in a data file were normalized to the time duration of the data file, to result in a value for counts  $\text{s}^{-1}$  1,280  $\text{mm}^{-2}$ . Due to the lack of spatial resolution of the system, some counts in each ROI may have come from the

opposite part of the plant, but given the close geometry and solid angle considerations, the fraction of the total is small. A total of eleven plants were imaged in the UCD-SPI system, three *A. thaliana*, and four each of the *A. halleri* genotypes.

### 2.3 | Quantification of Zn remaining in growth media after imaging

At the end of plant imaging, two values were recorded from an electronic pulse counter unit (Tennelec TC512 Dual Counter Timer) for the overall trigger rate of the system: the final rate with the plant in place in the system, and the rate with the plant removed (but the growth media still remaining in the holder). Measurements of the plant components in the well counter were made post-imaging, but due to the low activity levels (often 2  $\mu\text{Ci}$  or lower), the measurements were not stable above background.

Parallel resupply experiments with no radiolabel were done in triplicate to quantify the amount of Zn in the media before and after 24 hr resupply of 1  $\mu\text{M}$  Zn, and hence the ability of the plants to deplete Zn from their growth media. The Zn concentration in the growth media samples were quantified using ICP-AES analysis (UC Davis Analytical Lab). The resupply experiments without radiolabel were carried out in Magenta boxes in the growth chamber for a 24 hr period.

### 2.4 | Quantification of transport from imaging data

Absolute sensitivity of the system is known from measurement with a centrifuge tube containing known  $^{65}\text{Zn}$  activity. The calibrated system performance as measured with point gamma ray sources of a variety of energies broadly agrees with expectations from detailed calculations and simulations (Walker, Cherry, & Mitchell, 2014; Walker et al., 2015).

### 2.5 | Gamma-ray image data processing

The quantification measurements for regions of interest (ROIs) provide a count of average gamma-rays detected  $\text{s}^{-1} 1,280 \text{ mm}^{-2}$  (these units are used since both ROIs are of that area on the face of the detector). High levels of gamma rays were detected during the early time points, especially in *A. halleri*, and the gamma ray levels dissipated to a local minima around 3 hr. In order to compare the dynamics of the Zn transport from root to shoot across the samples, the shoot ROI measurements were normalized to the local minima by subtraction. To calculate the rate of transport of Zn into the shoot ROI, the initial slopes of gamma ray build up for shoot ROI were calculated with the time points between 3 hr and 24 hr. To carry out a comparison of time points where the first differences in Zn accumulation into shoot could be observed, the data needed to be processed further. The imaging setup collects  $8 \times 10^6$  gamma-rays (over a typical time period of 1,800 s) which summed together then constitutes a time point. Due to the difference in rates for each plant imaged, the time points for imaging are not matched sample to sample. In order to compare specific time points between the samples,

values for 3 hr, 4 hr, 5 hr, and so on until 12 hr, were calculated using the two adjacent time points. This was done by calculating the slope and intercept between each pair of time points. Zn signal for each interpolated time point ( $x$ ) was calculated using the formula  $y = mx + b$  (where  $m$  = slope and  $b$  = intercept from the values of two adjacent time points). Statistical analyses and time course plots were done in R version 3.4.2 (R Core Team, 2017) using *agricolae* (de Mendiburu, 2017), *lsmeans* (Lenth, 2016) and *ggplot2* (Wickham, 2016) packages and *wesanderson* palette (Ram & Wickham, 2015).

## 3 | RESULTS

### 3.1 | Dynamics of $\text{Zn}^{2+}$ movement in *A. halleri* vs. *A. thaliana*

The dynamics of Zn uptake and movement after Zn deprivation were visualized in vivo in intact plants of *Arabidopsis halleri* wild type (accession Langelshheim), the *A. halleri* AhHMA4-RNAi line 4.2.1 (in the Langelshheim accession background), and *A. thaliana* Col-0. First, the two species were grown to mature vegetative stage. *A. halleri* cuttings were grown hydroponically for 14 days to allow them to root. *A. thaliana* was grown on soil for 18 days, rinsed and transferred to Zn deprivation media (Hoagland media with no added  $\text{ZnSO}_4$ ) for hydroponic growth. The plants were allowed to acclimate to Zn deprivation for 19–21 days. ICP-AES analysis of the Zn deprivation media showed that Zn concentration of the media lacking any added Zn was 0.12  $\mu\text{M}$  and is thus considered low zinc media. Immediately prior to imaging, the plants were transferred to resupply media with 1  $\mu\text{M}$   $\text{ZnSO}_4$  (normal concentration of  $\text{ZnSO}_4$  in Hoagland media and control concentration in (Talke, Hanikenne, & Krämer, 2006)) and with 5.6–7.2 nM radioactive  $^{65}\text{Zn}$ . The plants were on the radiolabelled resupply media for 60 min, after which they were rinsed three times with non-radiolabelled resupply media before placing them on fresh non-radiolabeled resupply media for imaging with the UCD-SPI system. The time at which a plant was placed in the imaging system is considered the 0 hr time point (Figures 1 and 2). Zn signal was measured in both the root region of interest ("root ROI", blue box, Figure 1) and in the shoot region of interest ("shoot ROI", red box, Figure 1). In *A. halleri* wild-type plants, the signal was detected in the root at 0 hr, and then gradually moved up toward the shoot visibly at 12 hr and 24 hr, and subsequently appeared stationary in the upper part of the root from 36 hr to 60 hr (Figure 1a). In *A. halleri* HMA4-RNAi plants, the total gamma-ray signal never moved upwards from the root ROI, and instead moved slightly downwards in the root ROI over time, and the signal weakened considerably between 0 hr and 12 hr (Figure 1b). In *A. thaliana* wild-type plants, similarly to *A. halleri* HMA4-RNAi plants, no root-to-shoot movement of gamma-ray signal was visible, and the signal dissipated along the time course (Figure 1c). The radioactive signal in both the shoot and the root ROI started at their maximum for all *A. halleri* samples (Figure 2a, Supporting Information Figure S1), and reduced to a local minimum at approximately 3 hr. This effect is likely attributable to loosely bound  $^{65}\text{Zn}$  in the root apoplast, which is gradually desorbed into



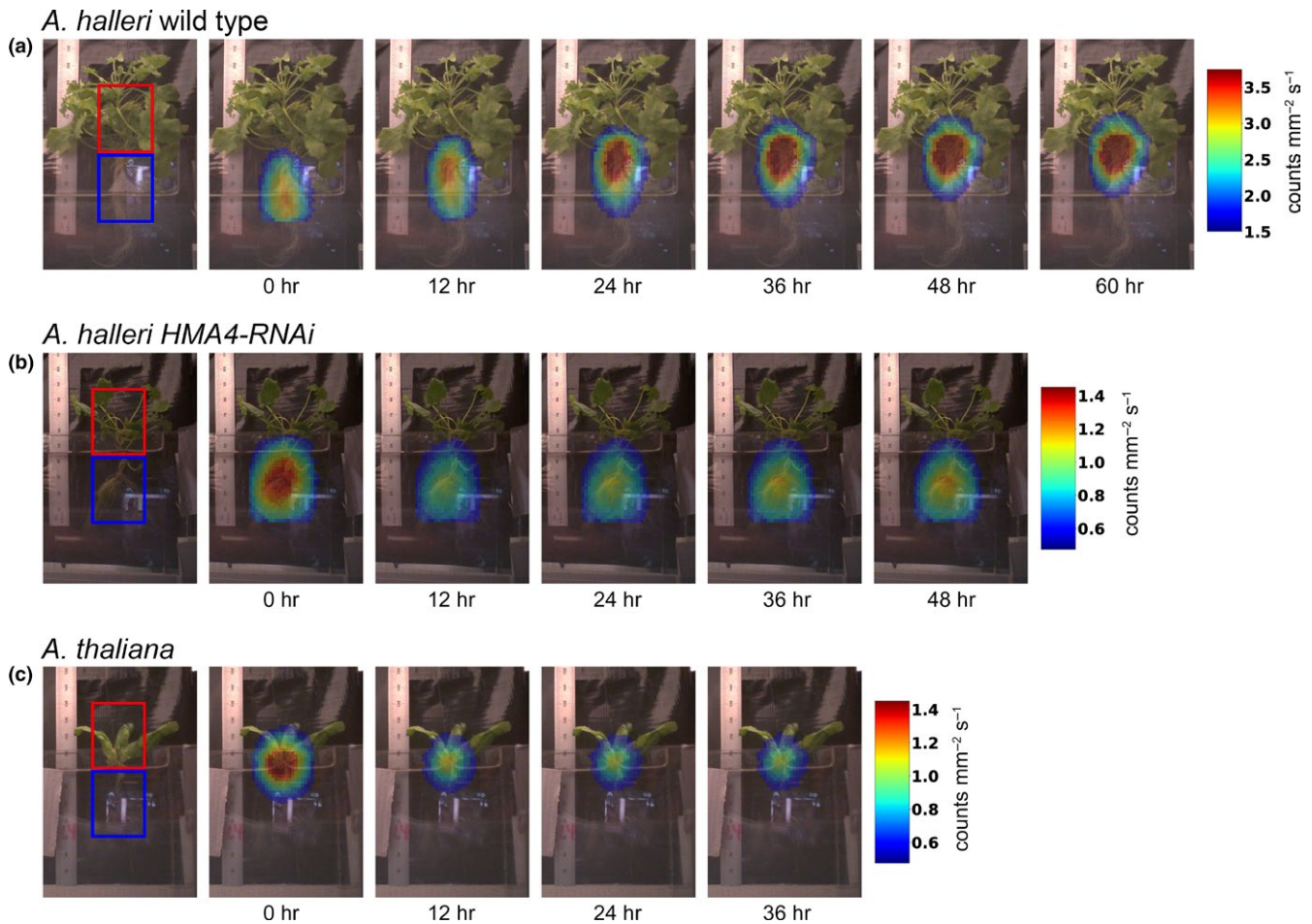


**FIGURE 1** Visualization of whole-plant Zn resupply dynamics as detected by UCD-SPI. Zn dynamics were measured for *Arabidopsis halleri* wild type (a), *A. halleri* HMA4-RNAi (b) and *Arabidopsis thaliana* Col-0 (c) plants upon Zn resupply ( $1 \mu\text{M}$   $\text{ZnSO}_4$ ) after 3 week Zn deprivation. Processed gamma ray detection data is overlaid with static pictures of the plants from which the data were collected. The red square represents the shoot ROI, and the blue square represents the root ROI

the external solution, thereby leaving the center of the field of view and reducing the likelihood of an emitted gamma ray being detected in the imaging system. In order to quantify and investigate root-to-shoot Zn transport dynamics, the focus was on the timepoints after the local minima, thus measurements were normalized to the time point at which the detected signal was the lowest close to 3 hr. Shoot data corrected for the local minima is shown in Figure 2b.

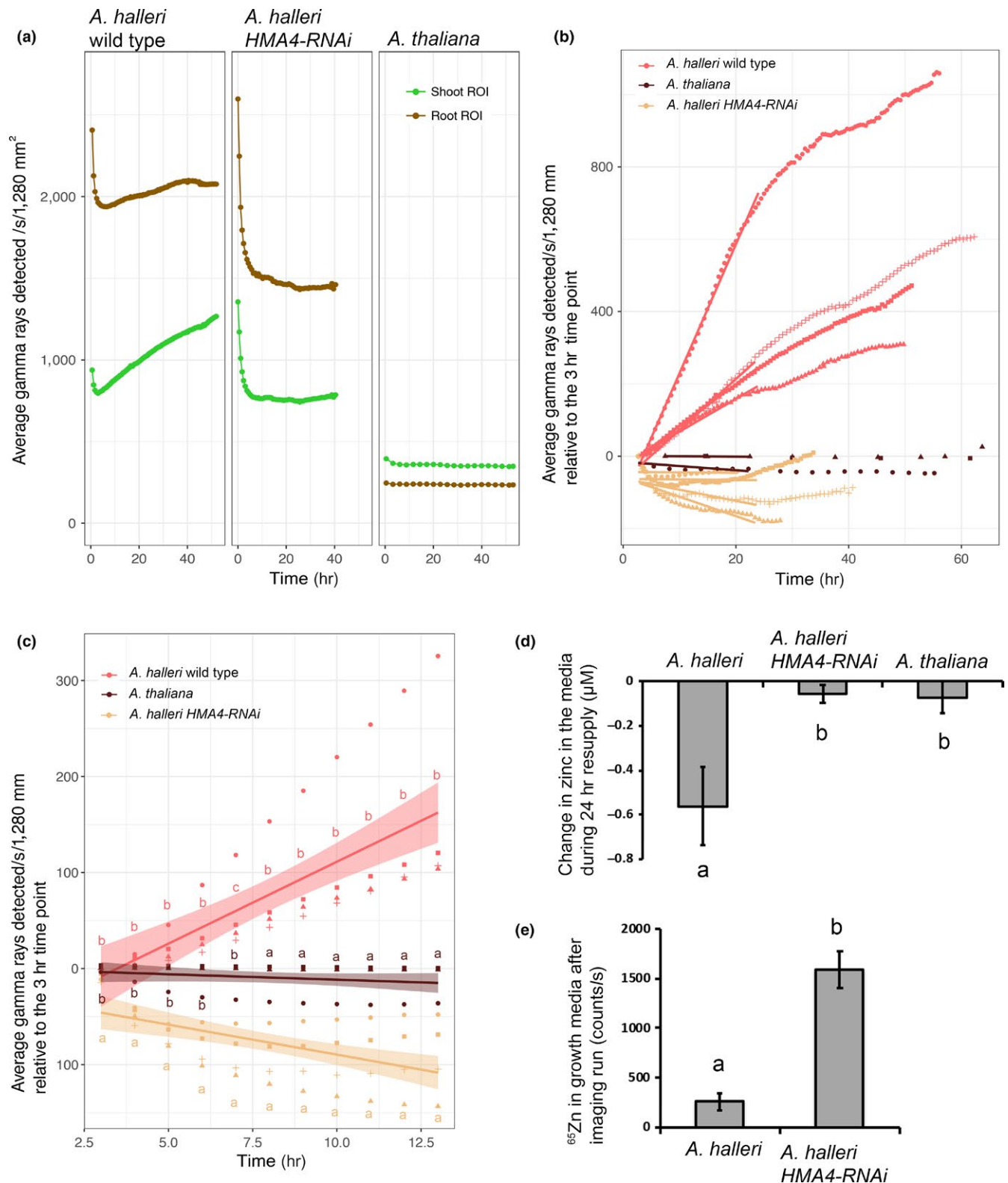
At the interpolated time points after 3 hr of resupply of radio-labeled Zn, a continuous linear relative increase in the amount of  $^{65}\text{Zn}$  was observed in the shoot of *A. halleri* wild-type plants (Figure 2c). By contrast, in both *A. halleri* HMA4-RNAi and *A. thaliana* shoots, no additional  $^{65}\text{Zn}$  accumulated over the time period examined. On the contrary, the *A. halleri* HMA4-RNAi shoots lost further  $^{65}\text{Zn}$  signal after the initial local minimum, and from 7 hr onwards this was statistically significant (Tukey's HSD test,  $p < 0.05$ ). The differential net ability of the three genotypes to take up Zn from the growth medium was determined through independent Zn resupply experiments. These experiments were conducted over the identical time period (24 hr) to the gamma ray imaging experiment, but ICP-AES was used to measure the amount of Zn remaining in the growth media (Figure 2d).

These data demonstrated that also at the whole-plant level, *A. halleri* wild-type plants took up significantly more Zn from the growth media than *A. halleri* HMA4-RNAi and *A. thaliana* (Figure 2d).

The root ROIs were also analyzed for change in  $^{65}\text{Zn}$  levels (Supporting Information Figure S2). All three genotypes had identically no change in the  $^{65}\text{Zn}$  signal across the analyzed time course (Tukey's HSD test).

### 3.2 | Silencing of HMA4 completely abolishes root-to-shoot transport of Zn and results in Zn extrusion

In our whole-plant imaging system, the *A. halleri* HMA4 RNAi line, shoot  $^{65}\text{Zn}$  levels in fact decreased over a 24 hr time period (Figure 2b-c, Tukey's HSD test,  $p < 0.05$ ). Finally, the amount of  $^{65}\text{Zn}$  signal remaining in the growth media after the imaging run is six-fold higher after imaging of *A. halleri* HMA4-RNAi compared to wild-type *A. halleri* (Figure 2e), indicating a higher net loss of  $^{65}\text{Zn}$  from the *A. halleri* HMA4 RNAi root into the surrounding media. This  $^{65}\text{Zn}$  represents Zn that was transferred into the imaging setup with the plant after the  $^{65}\text{Zn}$  treatment and root rinsing.



## 4 | DISCUSSION

### 4.1 | Advantages of gamma-ray imaging in intact plants

Aspects of metal uptake and homeostasis in plants may be understood well at the molecular level, but understanding of the

whole-plant dynamics has lagged behind due to the limitations of traditional experimental approaches and imaging systems. Radiolabeled molecules are widely used to measure the transport dynamics in biological systems. In experiments with whole plants and radiolabeled molecules, the biodistribution of the radiolabel is most typically analyzed by plant dissection and counting in a well counter, and for

**FIGURE 2** Quantification of Zn root-to-shoot transport dynamics. (a) Examples of raw data points for shoot (green) and root (brown) ROI measurements across the imaging time lapse (average gamma-rays detected  $1,280 \text{ mm}^{-2} \text{ s}^{-1}$ ). For *Arabidopsis halleri* wild type and the *A. halleri* HMA4-RNAi line, the 0 hr time point shows a high level of gamma-ray detection that dissipates to a local minimum at 3 hr. (b) Gamma-rays in the shoot normalized to the 3 hr local minima of the shoot ROI. In order to compare the dynamics of the  $^{65}\text{Zn}$  transport to the shoot across the samples, the values were normalized to the local minima. The slopes represent the rate of signal intensity change over time transport from 3 hr to 24 hr. The initial slopes are significantly steeper in *A. halleri* wild type compared to the two other genotypes (ANOVA, TukeyHSD,  $p = 0.0126$ ). Pink data points: *A. halleri* wild type. Beige data points: *A. halleri* HMA4-RNAi. Brown data points: *A. thaliana*. Different symbol shapes indicate replicates ( $n = 4$  for *A. halleri* wild type and *A. halleri* HMA4-RNAi,  $n = 3$  for *Arabidopsis thaliana*). (c) Gamma-rays visualized in shoots as in (B), displayed at discrete interpolated time points. The gamma-ray imaging setup collects  $8 \times 10^6$  gamma-rays which then constitute a time point. Due to this, the time points for imaging are not matched sample to sample. In order to compare specific time points between the samples, values for 3 hr, 4 hr, 5 hr, and so on until 12 hr, were interpolated using the two adjacent time points. The letters indicate samples that are significantly different between genotypes at each time point ( $p < 0.05$ , least-squares means). Lines represent the means and smoothed areas standard errors for each genotype. (d) Analytic ICP-AES quantification of Zn in resupply media after 24 hr resupply compared to 0 hr. E: Gamma-rays detected in the imaging media after plant imaging (average gamma-rays detected  $\text{s}^{-1} 1,280 \text{ mm}^{-2}$ ). As there is no radiolabeled  $^{65}\text{Zn}$  in the imaging media prior to when the plant is placed for imaging, this represents radiolabeled  $^{65}\text{Zn}$  leached from the plant into the media. Letters (in panels d, e) indicate significant differences ( $p < 0.05$ , Student's t-test) and error bars (panels d, e) indicate standard error

$\beta$ -emitters, by ashing the plant biomass and counting the radiolabel with a liquid scintillation counter. Several whole plant positron emission tomography (PET) imaging systems have been developed using  $^{11}\text{C}$  (Jahnke et al., 2009; Kawachi et al., 2011; Weisenberger et al., 2009), other groups have developed large scanners for  $\beta$ -imaging using  $^{32}\text{P}$  (Kanno et al., 2007), and autoradiography has been used to image radioisotope distribution of whole plants (Page & Feller, 2005). A scanner (Kawachi et al., 2011) has been used to perform PET imaging of  $^{65}\text{Zn}$  and  $^{107}\text{Cd}$  in rice plants (Fontanili et al., 2016; Suzui, Yin, Ishii, Sekimoto, & Kawachi, 2017). Each of these nuclear imaging methods has drawbacks: for  $\beta$ -imaging, the range of  $\beta$ -particles can be too short to escape the plant; for PET, radioisotope lifetimes are short and the range of the positron can be too long for a thin, low density plant, limiting the yield of annihilation gamma-rays; and autoradiography is invasive and can require exposure times of weeks or months. Therefore, UCD-SPI for nuclear imaging of gamma-ray emitters in plants has significant opportunity to contribute in a new way to transport studies. Indeed, the UCD-SPI system has extremely high sensitivity ( $\sim 10\%$ ) for a single-photon imaging system, orders of magnitude higher than is found for SPECT systems used in medical imaging (often  $\sim 0.01\%$ ). This is extremely useful for imaging over long periods of time with high energy gamma rays, as it allows for imaging very low levels of radiotracer and thereby eases the practical issues of radiation safety and shielding and waste generation.

In particular, the uniquely high sensitivity of the system means that very small amounts (nCi) of radioisotopes may be imaged and followed over time. The system used here had the advantage that one entire time course can be recorded on a single plant. In time courses involving destructive sampling or imaging, data for the different time points are from distinct plant individuals, which generates substantial noise. This is particularly disruptive in experiments with non-model plants such as *A. halleri*, which show substantially larger variation in plant architecture between independently grown plants even of an identical genotype.

Common PET isotopes of interest for plant studies include several found in organic compounds:  $^{11}\text{C}$  ( $T_{1/2} = 20 \text{ min}$ ),  $^{13}\text{N}$  ( $T_{1/2} = 10 \text{ min}$ ), and  $^{18}\text{F}$  ( $T_{1/2} = 109 \text{ min}$ ). These atoms can be

substituted into amino acids or sugars in plants to follow the natural in situ processes (Cherry, Sorenson, & Phelps, 2003). However, due to the short lifetimes of PET radioisotopes, only short biological processes, such as photosynthesis, may be imaged. In contrast, single gamma-ray emitting radiotracers used in single photon emission computed tomography (SPECT) are typically metals and do not easily label organic molecules. However, many trace element metals are essential to a plant's survival (Clemens, 2001; Williams, Pittman, & Hall, 2000). An active area of plant research is studying hyperaccumulation of metals in plants using a radioisotope of that metal; commonly studied metals include: Cd, Zn, Mn, Co, and Ni (Krämer, 2010; Page & Feller, 2005). Other potential applications for SPECT imaging include: studying plant ion transport in xylem (Macklon, 1970; Ueno et al., 2008), studying metabolic processes such as tracers for phloem transport (Omid, Malter, Peleg, & Wolf, 2008), and studying signaling by labeled exogenous peptides or proteins (Santner & Estelle, 2009). One further advantage of imaging systems based on gamma-ray detection is the possibility of detecting the interactions of multiple radioisotopes simultaneously as the gamma-rays that they emit have distinct energies that can be distinguished from each other by the detector. For example, simultaneous imaging of  $^{65}\text{Zn}$  (gamma-ray 1,116 keV) and  $^{109}\text{Cd}$  (22 keV) would enable teasing apart the competition dynamics in their uptake.

However, there is an inherent tradeoff in increased sensitivity of the UCD-SPI system with spatial resolution. Spatial resolution at the mm-scale could be obtained using a collimator to better define the spatial origin of detected gamma rays, but this would lead to a greatly reduced event rate in the system. For the high-energy gamma rays of  $^{65}\text{Zn}$ , collimation is a particular challenge. Given the hours-long time scale of the transport studied here, it is possible that the choice of a collimator could have provided improved event positioning while preserving a usable event rate. A possible hybrid approach could have included using an insertable/removable collimator to acquire an alternating combination of two types of images: high sensitivity-low spatial resolution without the collimator; and low sensitivity-higher spatial resolution with a collimator. However, the use of a collimator for this system is unexplored thus far.



## 4.2 | Zn transport dynamics in *A. halleri* and *A. thaliana*

Zn uptake into the symplast in the outer root layers and loading into the apoplastic xylem stream are well understood on molecular level (Moreira, Moraes, & dos Reis, 2018). However, the dynamics of symplastic movement and patterning of the radial transport have thus far only been modeled to elucidate the timescales of these events (Claus et al., 2013). After xylem loading, the mass flow-mediated movement of Zn into the shoot inside the xylem is expected to occur within 30 min in *Arabidopsis*, as previously shown for water (Park et al., 2014) and Cd in xylem sap (Ueno et al., 2008). From previous SPECT imaging, we have shown that a pulse of radiolabelled pertechnetate ( $^{99m}\text{TcO}_4^-$ ) moving in the xylem stream reaches the shoot apical meristem of a 2 week old sunflower already in 5 min (Walker et al., 2015).

The rate-limiting step for root-to-shoot translocation of Zn was proposed to be xylem loading involving HMA4 transporters in both *A. halleri* and *A. thaliana* (Hanikenne et al., 2008; Sinclair, Sherson, Jarvis, Camakaris, & Cobbett, 2007). The dynamics of root-to-shoot Zn flux, however, have so far remained unclear in different species and transgenic lines. Estimates of Zn translocation rates from root to shoot were first obtained by spectroscopy methods of ashed shoot tissues. Early work with metal hyperaccumulator *Noccaea caerulea* suggested that the speed of root-to-shoot Zn transport was between 20 and 60 hr (Lasat, Baker, & Kochian, 1996; Lombi, Zhao, McGrath, Young, & Sacchi, 2001). Recently, positron imaging of Zn uptake estimated the time for Zn root-to-panicle transport in dwarfed mature rice to be 5.3 hr (Suzui et al., 2017). Here, we have produced the first Zn root-to-shoot imaging data for *A. halleri* using UCD-SPI. Zn accumulates within the shoot of *A. halleri*, consistent with its ability to hyperaccumulate Zn, different from the *HMA4* RNAi line. The speed of Zn transport into the shoot in our data as observed with the smoothed standard error show clear shoot accumulation within 5–7 hr, respectively (Figure 2c). These results are in line with previous reports for rice (Suzui et al., 2017). This contrasts strongly with the faster speed of the other xylem-transported compounds, such as water in *A. thaliana* (Park et al., 2014), Cd in *A. halleri* (Ueno et al., 2008) and pertechnetate in sunflower (Walker et al., 2015), all measured to reach the shoot in 30 min. It should be noted, however, that the experiments demonstrating water transport (Park et al., 2014) and Cd transport (Ueno et al., 2008) were carried out using decapitated stems and are thus destructive in nature, but also far more sensitive to small quantities than the method used here. The slower speed of Zn transport indicates that Zn loading into the xylem by HMA4 is slow and under tight control even in the metal hyperaccumulator *A. halleri*. Modelling the radial transport of Zn uptake has indeed indicated that HMA concentration is one of the key determinants of the uptake dynamics (Claus et al., 2013).

The HMA4 transporter pumps  $\text{Zn}^{2+}$  from the root symplast into the apoplastic xylem sap of *A. thaliana* (Verret et al., 2004). Strongly elevated expression of *A. halleri* HMA4 was suggested to be responsible for the increased in root-to-shoot translocation of Zn in *A. halleri* relative to *A. thaliana* (Hanikenne et al., 2008). This conclusion was drawn based

on the quantification of shoot Zn concentrations after long-term growth in *HMA4*-RNAi lines and wild-type *A. halleri* and in *A. thaliana* Col-0 (Hanikenne et al., 2008). In the same experiment, root Zn concentration was elevated in some *A. halleri* *HMA4* RNAi lines relative to *A. halleri* wild-type plants and even relative to *A. thaliana* (Hanikenne et al., 2008).

HMA4 is critical to the ability of *A. halleri* to hyperaccumulate Zn. We tested the functional role of HMA4 for *A. halleri* Zn translocation from root to shoot by imaging the Zn uptake dynamics of *A. halleri* *HMA4*-RNAi line relative to *A. halleri*. We found that the Zn signal in the shoot of *HMA4*-RNAi line did not increase over our 40-hr imaging period, but conversely, we saw a continuous decrease in shoot Zn signal with significant differences observable at 3 hr (Figure 2c). The lack of an increase in shoot Zn confirms that Zn loading into the xylem is abolished in the *HMA4*-RNAi plants (Hanikenne et al., 2008). The continuous decrease in the Zn signal in the shoot ROI seems to reflect bleeding of the strong early Zn signal from the root ROI into the shoot ROI. The dissipating signal through the *A. halleri* *HMA4*-RNAi time course could be due to apoplastic  $^{65}\text{Zn}$  adsorbed to the cell walls of outer root layers during the  $^{65}\text{Zn}$  pulse (Lasat et al., 1996) and not removed by the triple rinsing with Hoagland solution. This cell wall-adsorbed  $^{65}\text{Zn}$  would be desorbed into the growth medium during the imaging period by diffusion. The influx of Zn into the root symplast is very tightly and rapidly regulated in Zn-concentration dependent fashion (Claus et al., 2013; van de Mortel et al., 2006; Talke et al., 2006). Without the loading of Zn into the xylem, Zn builds up in the root symplast. In the case of *A. halleri* *HMA4*-RNAi, the symplast could be saturated with Zn at 3 hr after the resupply, leading to prevention of further uptake of the cell wall-adsorbed  $^{65}\text{Zn}$  and thus higher Zn desorption than Zn uptake into the symplast.

Finally, we compared the dynamics of Zn movement in the Zn hyperaccumulator *A. halleri* with those in the related species *A. thaliana*, a non-metal hyperaccumulator. Based on previous studies comparing Zn-deficient to Zn-sufficient plants of *A. thaliana* and/or *A. halleri*, the Zn concentrations in our hydroponic solutions can be estimated to result in moderate Zn deficiency (Talke et al., 2006; Sinclair et al., 2018). The net concentration of  $^{65}\text{Zn}$  in the resupply media over the 24 hr period showed a net decrease, suggesting that Zn was taken up into the shoot, although these levels are variable. We found that Zn resupply after Zn deprivation in *A. thaliana* did not lead to detectable uptake or change of Zn in the shoot or the root ROI. It is possible that the small size and flat rosette growth habit of *A. thaliana* affected our ability to detect Zn dynamics. Also, low abundance of HMA4 transporters in *A. thaliana* roots may lead to much slower dynamics that we were unable to capture. In the absence of quantification of  $^{65}\text{Zn}$  levels in the shoot, it is possible, although unlikely, that Zn was not translocated in *A. thaliana*.

The heavy metal imaging study presented here is of interest for phytoremediation applications (Kärenlampi et al., 2000; Krämer, 2010; Robinson et al., 1998; Salt, Smith, & Raskin, 1998; Sarma, 2011). Although most plants prevent the accumulation of heavy metals so as to avert toxicity, metal hyperaccumulators selectively extract high concentrations of metals from the soil into their shoots without incurring symptoms of toxicity (Baker & Brooks, 1989; Frérot et al., 2010). By using the heavy metal radiolabel  $^{65}\text{Zn}$  and the





UCD-SPI imaging system, we gained a more detailed spatiotemporal understanding of the dynamics of metal movement into plants, which may be a path toward the use and understanding of metal hyperaccumulating plants for such advantageous applications.

## ACKNOWLEDGMENTS

KK was supported by Finnish Cultural Foundation postdoctoral fellowship. K LW was supported by Office of Science (BER), U.S. Department of Energy. SMB was partially funded as an HHMI Faculty Scholar.

## CONFLICT OF INTEREST

The authors declare no conflict of interest associated with the work described in this manuscript.

## AUTHOR CONTRIBUTIONS

KK, GM, UK, SC, and SB designed the research; KK, KW, and GM performed research; KW and GM contributed new analytic/computational/etc. tools; KK, KW, GM, SC, and SB analyzed data, and KK, GM, and SB wrote the paper.

## ORCID

Kaisa Kajala  <https://orcid.org/0000-0001-6483-7473>

Katherine L. Walker  <https://orcid.org/0000-0001-7874-4278>

Gregory S. Mitchell  <https://orcid.org/0000-0002-8276-1107>

Ute Krämer  <https://orcid.org/0000-0001-7870-4508>

Simon R. Cherry  <https://orcid.org/0000-0002-0155-5644>

Siobhan M. Brady  <https://orcid.org/0000-0001-9424-8055>

Kaisa Kajala  <https://orcid.org/0000-0001-6483-7473>

## REFERENCES

- Baker, A. J. M., & Brooks, R. R. (1989). Terrestrial higher plants which hyperaccumulate metallic elements - A review of their distribution, ecology and phytochemistry. *Biorecovery*, 1, 81–126.
- Becher, M., Talke, I. N., Krall, L., & Krämer, U. (2004). Cross-species microarray transcript profiling reveals high constitutive expression of metal homeostasis genes in shoots of the zinc hyperaccumulator *Arabidopsis halleri*. *The Plant Journal: For Cell and Molecular Biology*, 37, 251–268. <https://doi.org/10.1046/j.1365-313X.2003.01959.x>
- Bert, V., Macnair, M. R., de Laguerie, P., Saumitou-Laprade, P., & Petit, D. (2000). Zinc tolerance and accumulation in metallicolous and nonmetallicolous populations of *Arabidopsis halleri* (Brassicaceae). *The New Phytologist*, 146, 225–233. <https://doi.org/10.1046/j.1469-8137.2000.00634.x>
- Bert, V., Meerts, P., Saumitou-Laprade, P., Salis, P., Gruber, W., & Verbruggen, N. (2003). Genetic basis of Cd tolerance and hyperaccumulation in *Arabidopsis halleri*. *Plant and Soil*, 249, 9–18. <https://doi.org/10.1023/A:1022580325301>
- Cherry, S. R., Sorenson, J. A., & Phelps, M. E. (2003). *Physics in nuclear medicine*, 3rd ed. Philadelphia, PA: Saunders.
- Claus, J., Bohmann, A., & Chavarria-Krauser, A. (2013). Zinc uptake and radial transport in roots of *Arabidopsis thaliana*: A modelling approach to understand accumulation. *Annals of Botany*, 112, 369–380. <https://doi.org/10.1093/aob/mcs263>
- Clemens, S. (2001). Molecular mechanisms of plant metal tolerance and homeostasis. *Planta*, 212, 475–486. <https://doi.org/10.1007/s004250000458>
- Courbot, M., Willems, G., Motte, P., Arvidsson, S., Roosens, N., Saumitou-Laprade, P., & Verbruggen, N. (2007). A major quantitative trait locus for cadmium tolerance in *Arabidopsis halleri* colocalizes with HMA4, a gene encoding a heavy metal ATPase. *Plant Physiology*, 144, 1052–1065. <https://doi.org/10.1104/pp.106.095133>
- Deinlein, U., Weber, M., Schmidt, H., Rensch, S., Trampczynska, A., Hansen, T. H., ... Clemens, S. (2012). Elevated nicotianamine levels in *Arabidopsis halleri* roots play a key role in zinc hyperaccumulation. *The Plant Cell*, 24, 708–723.
- Fontanilli, L., Lancilli, C., Suzui, N., Dendena, B., Yin, Y.-G., Ferri, A., ... Nocito, F. F. (2016). Kinetic analysis of zinc/cadmium reciprocal competitions suggests a possible Zn-insensitive pathway for root-to-shoot cadmium translocation in rice. *Rice*, 9, 16.
- Frérot, H., Faucon, M.-P., Willems, G., Godé, C., Courseaux, A., Darracq, A., ... Saumitou-Laprade, P. (2010). Genetic architecture of zinc hyperaccumulation in *Arabidopsis halleri*: The essential role of QTL × environment interactions. *The New Phytologist*, 187, 355–367. <https://doi.org/10.1111/j.1469-8137.2010.03295.x>
- Grotz, N., Fox, T., Connolly, E., Park, W., Gueriot, M. L., & Eide, D. (1998). Identification of a family of zinc transporter genes from *Arabidopsis* that respond to zinc deficiency. *Proceedings of the National Academy of Sciences*, 95, 7220–7224. <https://doi.org/10.1073/pnas.95.12.7220>
- Hanikenne, M., & Nouet, C. (2011). Metal hyperaccumulation and hyper-tolerance: A model for plant evolutionary genomics. *Current Opinion in Plant Biology*, 14, 252–259. <https://doi.org/10.1016/j.pbi.2011.04.003>
- Hanikenne, M., Talke, I. N., Haydon, M. J., Lanz, C., Nolte, A., Motte, P., ... Krämer, U. (2008). Evolution of metal hyperaccumulation required cis-regulatory changes and triplication of HMA4. *Nature*, 453, 391–395. <https://doi.org/10.1038/nature06877>
- Hussain, D., Haydon, M. J., Wang, Y., Wong, E., Sherson, S. M., Young, J., ... Cobbett, C. S. (2004). P-type ATPase heavy metal transporters with roles in essential zinc homeostasis in *Arabidopsis*. *The Plant Cell*, 16, 1327–1339.
- Isaure, M.-P., Fayard, B., Sarret, G., Pairis, S., & Bourguignon, J. (2006). Localization and chemical forms of cadmium in plant samples by combining analytical electron microscopy and X-ray spectromicroscopy. *Spectrochimica Acta. Part B: Atomic Spectroscopy*, 61, 1242–1252. <https://doi.org/10.1016/j.sab.2006.10.009>
- Jahnke, S., Menzel, M. I., van Dusschoten, D., Roeb, G. W., Bühler, J., Minwyelet, S., ... Schurr, U. (2009). Combined MRI-PET dissects dynamic changes in plant structures and functions. *The Plant Journal: For Cell and Molecular Biology*, 59, 634–644.
- Kanno, S., Rai, H., Ohya, T., Hayashi, Y., Tanoi, K., & Nakanishi, T. M. (2007). Real-time imaging of radioisotope labeled compounds in a living plant. *Journal of Radioanalytical and Nuclear Chemistry*, 272, 565–570. <https://doi.org/10.1007/s10967-007-0625-z>
- Kärenlampi, S., Schat, H., Vangronsveld, J., Verkleij, J. A. C., van der Lelie, D., Mergeay, M., & Tervahauta, A. I. (2000). Genetic engineering in the improvement of plants for phytoremediation of metal polluted soils. *Environmental Pollution*, 107, 225–231. [https://doi.org/10.1016/S0269-7491\(99\)00141-4](https://doi.org/10.1016/S0269-7491(99)00141-4)
- Kawachi, N., Kikuchi, K., Suzui, N., Ishii, S., Fujimaki, S., Ishioka, N. S., & Watabe, H. (2011). Imaging of carbon translocation to fruit using carbon-11-labeled carbon dioxide and positron emission tomography. *IEEE Transactions on Nuclear Science*, 58, 395–399. <https://doi.org/10.1109/TNS.2011.2113192>
- Krämer, U. (2010). Metal hyperaccumulation in plants. *Annual Review of Plant Biology*, 61, 517–534. <https://doi.org/10.1146/annurev-arplant-042809-112156>



- Krämer, U., Talke, I. N., & Hanikenne, M. (2007). Transition metal transport. *FEBS Letters*, 581, 2263–2272. <https://doi.org/10.1016/j.febslet.2007.04.010>
- Lanquar, V., Grossmann, G., Vinkenborg, J. L., Merckx, M., Thomine, S., & Frommer, W. B. (2014). Dynamic imaging of cytosolic zinc in Arabidopsis roots combining FRET sensors and RootChip technology. *The New Phytologist*, 202, 198–208. <https://doi.org/10.1111/nph.12652>
- Lasat, M. M., Baker, A. J. M., & Kochian, L. V. (1996). Physiological characterization of root Zn<sup>2+</sup> absorption and translocation to shoots in Zn hyperaccumulator and nonaccumulator species of *Thlaspi*. *Plant Physiology*, 112, 1715–1722. <https://doi.org/10.1104/pp.112.4.1715>
- Lenth, R. V. (2016). Least-squares means: The R package lsmeans. *Journal of Statistical Software*, 69, 1–33. <https://doi.org/10.18637/jss.v069.i01>
- Lombi, E., Zhao, F. J., McGrath, S. P., Young, S. D., & Sacchi, G. A. (2001). Physiological evidence for a high-affinity cadmium transporter highly expressed in a *Thlaspi caerulescens* ecotype. *The New Phytologist*, 149, 53–60. <https://doi.org/10.1046/j.1469-8137.2001.00003.x>
- Macklon, A. E. S. (1970). Electrochemical aspects of ion transport in plants. *Journal of the Science of Food and Agriculture*, 21, 178–181. [https://doi.org/10.1002/\(ISSN\)1097-0010](https://doi.org/10.1002/(ISSN)1097-0010)
- de, Mendiburu, F. (2017). *agricolae: Statistical Procedures for Agricultural Research*.
- Moreira, A., Moraes, L. A. C., & dos Reis, A. R. (2018). The molecular genetics of zinc uptake and utilization efficiency in crop plants. In M. A. Hossain, T. Kamiya, D. J. Burritt, L.-S. Phan Tran, & T. Fujiwara (Eds.), *Plant micronutrient use efficiency* (pp. 87–108). London, UK: Academic Press; Elsevier Inc. <https://doi.org/10.1016/B978-0-12-812104-7.00006-X>
- van de Mortel, J. E., Almar Villanueva, L., Schat, H., Kwekkeboom, J., Coughlan, S., Moerland, P. D., ... Aarts, M. G. M. (2006). Large expression differences in genes for iron and zinc homeostasis, stress response, and lignin biosynthesis distinguish roots of *Arabidopsis thaliana* and the related metal hyperaccumulator *Thlaspi caerulescens*. *Plant Physiology*, 142, 1127–1147. <https://doi.org/10.1104/pp.106.082073>
- Omid, A., Malter, D., Peleg, G., & Wolf, S. (2008). Long-distance trafficking of macromolecules in the phloem. *Plant Signaling and Behavior*, 3, 260–262. <https://doi.org/10.4161/psb.3.4.5196>
- Page, V., & Feller, U. (2005). Selective transport of zinc, manganese, nickel, cobalt and cadmium in the root system and transfer to the leaves in young wheat plants. *Annals of Botany*, 96, 425–434. <https://doi.org/10.1093/aob/mci189>
- Park, J., Kim, H. K., Ryu, J., Ahn, S., Lee, S. J., & Hwang, I. (2014). Functional water flow pathways and hydraulic regulation in the xylem network of Arabidopsis. *Plant and Cell Physiology*, 56, 520–531. <https://doi.org/10.1093/pcp/pcu198>
- Pauwels, M., Frérot, H., Bonnin, I., & Saumitou-Laprade, P. (2006). A broad-scale analysis of population differentiation for Zn tolerance in an emerging model species for tolerance study: *Arabidopsis halleri* (Brassicaceae). *Journal of Evolutionary Biology*, 19, 1838–1850. <https://doi.org/10.1111/j.1420-9101.2006.01178.x>
- Pollard, A. J., Reeves, R. D., & Baker, A. J. M. (2014). Facultative hyperaccumulation of heavy metals and metalloids. *Plant Science: An International Journal of Experimental Plant Biology*, 217–218, 8–17. <https://doi.org/10.1016/j.plantsci.2013.11.011>
- R Core Team. (2017). *R: A language and environment for statistical computing*. Vienna, Austria: R Foundation for Statistical Computing.
- Ram, K., & Wickham, H. (2015). *wesanderson: A Wes Anderson Palette Generator*.
- Ramesh, S. A., Shin, R., Eide, D. J., & Schachtman, D. P. (2003). Differential metal selectivity and gene expression of two zinc transporters from rice. *Plant Physiology*, 133, 126–134. <https://doi.org/10.1104/pp.103.026815>
- Robinson, B. H., Leblanc, M., Petit, D., Brooks, R. R., Kirkman, J. H., & Gregg, P. E. H. (1998). The potential of *Thlaspi caerulescens* for phytoremediation of contaminated soils. *Plant and Soil*, 203, 47–56. <https://doi.org/10.1023/A:1004328816645>
- Salt, D. E., Smith, R. D., & Raskin, I. (1998). Phytoremediation. *Annual Review of Plant Physiology and Plant Molecular Biology*, 49, 643–668. <https://doi.org/10.1146/annurev.arplant.49.1.643>
- Santner, A., & Estelle, M. (2009). Recent advances and emerging trends in plant hormone signalling. *Nature*, 459, 1071–1078. <https://doi.org/10.1038/nature08122>
- Sarma, H. (2011). Metal hyperaccumulation in plants: A review focusing on phytoremediation technology. *Journal of Environmental Science and Technology*, 4, 118–138. <https://doi.org/10.3923/jest.2011.118.138>
- Sinclair, S. A., Senger, T., Talke, I. N., Cobbett, C. S., Haydon, M. J., & Krämer, U. (2018). Systemic upregulation of MTP2- and HMA2-mediated Zn partitioning to the shoot supplements local Zn deficiency responses. *The Plant Cell*, 30, 2463–2479.
- Sinclair, S. A., Sherson, S. M., Jarvis, R., Camakaris, J., & Cobbett, C. S. (2007). The use of the zinc-fluorophore, Zinpyr-1, in the study of zinc homeostasis in Arabidopsis roots. *The New Phytologist*, 174, 39–45. <https://doi.org/10.1111/j.1469-8137.2007.02030.x>
- Suzui, N., Yin, Y.-G., Ishii, S., Sekimoto, H., & Kawachi, N. (2017). Visualization of zinc dynamics in intact plants using positron imaging of commercially available Zn. *Plant Methods*, 13, 40. <https://doi.org/10.1186/s13007-017-0188-0>
- Talke, I. N., Hanikenne, M., & Krämer, U. (2006). Zinc-dependent global transcriptional control, transcriptional deregulation, and higher gene copy number for genes in metal homeostasis of the hyperaccumulator *Arabidopsis halleri*. *Plant Physiology*, 142, 148–167. <https://doi.org/10.1104/pp.105.076232>
- Ueno, D., Iwashita, T.-J., Zhao, F., & Ma, J. F. (2008). Characterization of Cd translocation and identification of the Cd form in xylem sap of the Cd-hyperaccumulator *Arabidopsis halleri*. *Plant and Cell Physiology*, 49, 540–548. <https://doi.org/10.1093/pcp/pcn026>
- Verret, F., Gravot, A., Auroy, P., Leonhardt, N., David, P., Nussaume, L., ... Richaud, P. (2004). Overexpression of AtHMA4 enhances root-to-shoot translocation of zinc and cadmium and plant metal tolerance. *FEBS Letters*, 576, 306–312. <https://doi.org/10.1016/j.febslet.2004.09.023>
- Walker, K. L., Cherry, S. R., & Mitchell, G. S. (2014). Detector performance characterization for high sensitivity single-photon imaging. *IEEE Transactions on Nuclear Science*, 61, 1118–1125. <https://doi.org/10.1109/TNS.2014.2299494>
- Walker, K. L., Judenhofer, M. S., Cherry, S. R., & Mitchell, G. S. (2015). Un-collimated single-photon imaging system for high-sensitivity small animal and plant imaging. *Physics in Medicine and Biology*, 60, 403–420. <https://doi.org/10.1088/0031-9155/60/1/403>
- Weisenberger, A. G., Kross, B., McKisson, J., Stolin, A., Zorn, C., Howell, C. R., ... Smith, M. F. (2009). *Positron emission tomography detector development for plant biology*. 2009 IEEE Nuclear Science Symposium Conference Record (NSS/MIC). IEEE, 2323–2328.
- Wickham, H. (2016). *ggplot2: Elegant graphics for data analysis*. New York, NY: Springer-Verlag. <https://doi.org/10.1007/978-3-319-24277-4>
- Williams, L. E., Pittman, J. K., & Hall, J. L. (2000). Emerging mechanisms for heavy metal transport in plants. *Biochimica et Biophysica Acta (BBA) - Biomembranes*, 1465, 104–126. [https://doi.org/10.1016/S0005-2736\(00\)00133-4](https://doi.org/10.1016/S0005-2736(00)00133-4)

## SUPPORTING INFORMATION

Additional supporting information may be found online in the Supporting Information section at the end of the article.

**How to cite this article:** Kajala K, Walker KL, Mitchell GS, Krämer U, Cherry SR, Brady SM. Real-time whole-plant dynamics of heavy metal transport in *Arabidopsis halleri* and *Arabidopsis thaliana* by gamma-ray imaging. *Plant Direct*. 2019;3:1–10. <https://doi.org/10.1002/pld3.131>